Electronic Supplementary Material (ESI) for Journal of Materials Chemistry A.

This journal is © The Royal Society of Chemistry 2021

Supporting Information

Electroactive Single-Atom Copper Anchored MXene Nanohybrid Filter for Ultrafast Water Decontamination

Limin Jin,[a] Shijie You,[b]* Yuan Yao,[c] Hong Chen,[d] Yi Wang,[e] Yanbiao Liu[a]*

[a] Textile Pollution Controlling Engineering Center of Ministry of Environmental Protection, College of Environmental Science and Engineering, Donghua University, Shanghai 201620, China. E-mail: yanbiaoliu@dhu.edu.cn, Tel: +86 21 67798752.

[b] State Key Laboratory of Urban Water Resource and Environment, School of Environment, Harbin Institute of Technology, Harbin 150090, China. E-mail: sjyou@hit.edu.cn, Tel: +86 451 8628 2008.

[c] MIIT Key Laboratory of Critical Materials Technology for New Energy Conversion and Storage, School of Chemistry and Chemical Engineering, Harbin Institute of Technology, Harbin 150080, China.

[d] School of Environmental Science & Engineering, Southern University of Science and Technology, Shenzhen 518055, China.

[e] State Key Laboratory of NBC Protection for Civilian, Beijing 102205, China.

Supporting Information: 5 Texts, 2 Tables and 20 Figures

Text S1. Chemicals and reagents.

Ti_3AlC_2 powder were obtained from Jilin 11 Technology Co. Ltd. (China). Polytetrafluoroethylene (PTFE, 50 mm diameter with a pore size of 0.47 μm) was purchased from Millipore (USA). Potassium peroxymonosulfate (PMS, $2KHSO_5 \cdot KHSO_4 \cdot K_2SO_4$), sulfamethoxazole (SMX, 98%), carbamazepine (CBZ, 98%), tetracycline (TC, 98%) bisphenol A (BPA, 96%), levofloxacin (Lev, 97%), 1,3-diphenylisobenzofuran (DPBF, 97%), benzoic acid (BA, 99%), and *p*-hydroxybenzoic acid (HBA, 99%) were procured from Sigma-Aldrich (Shanghai, China). Sodium chloride (NaCl, 96%), sodium nitrate ($NaNO_3$, 99%), disodium hydrogen phosphate (Na_2HPO_4, 96%), sodium bicarbonate ($NaHCO_3$, 99.8%), 2,2,6,6-tetramethyl-4-piperidinol (TEMP, 96%), 5,5-dimethyl-1-pyrroline-n-oxide (DMPO, 97%), furfuryl alcohol (FFA, 98%), *tert*-butyl alcohol (TBA, 98%), methanol (98%), ethanol (C_2H_5OH, 96%), nitric acid (HNO_3, 65 wt%), lithium fluoride (LiF, 98%) hydrochloric acid (HCl, 36-38%), sodium hydroxide (NaOH, 96%) and hydrazine hydrate ($N_2H_4 \cdot H_2O$, 50%) were supplied by Sinopharm Chemical Reagent Co. Ltd. (China). All reagents were used without further purification. Deionized water (resistivity ≥18.2 MΩ cm^{-1}) was used in the experiments.

Text S2. Characterizations.

The morphology of the nanohybrid membrane was studied by field emission scanning electron microscopy (FESEM, JSM-7500F, Japan) and field emission transmission electron microscopy (FETEM, Talos F200S, USA). The topographical images of the $Ti_3C_2T_x$ nanosheets were recorded *via* atomic force microscopy (AFM, Bruker, USA) under tapping mode at ambient conditions. The images of the isolated single copper atoms and nanoclusters were obtained by using high-angle annular dark field-scanning transmission electron microscopy (HAADF-STEM, JEM-ARM200 F, Japan). The Cu K-edge X-ray adsorption fine structure (XAFS) analysis was carried out at the Beijing Synchrotron Irradiation Facility using the fluorescence mode. An X-ray diffractometer (XRD, D/max 2550 VB/PC, Japan) equipped with Cu Kα radiation (λ = 1.5418 Å) was used to analyze the phase structure of the catalysts. The composition and chemical state of the catalysts were characterized by X-ray photoelectron spectroscopy (XPS, Escalab 250 Xi, USA). The Raman spectra were collected using a micro-Raman spectroscopy system (inVia-Reflex, UK). Fourier transform infrared spectrometer (FT-IR, NEXUS-670, ThermoFisher, USA) was measured with KBr powder as the reference transmittance in a wavenumber range of 4000-400 cm^{-1} to analyze the functional groups of the filters. The total organic carbon (TOC) was determined using a TOC/TN analyzer (Multi N/C 3100, Germany). Inductively coupled plasma mass spectrometry (ICP-MS, iCAP-Q, USA) was used to determine the copper ions in the nanohybrid membrane and effluent. The flow rate was controlled by using an Ismatec ISM833C peristaltic pump (Switzerland). The electric field was developed by using a DH1766A-1 DC power supply system (China), and the electric current was measured using a multi-meter (Fluke 18B, China).

Text S3. Degradation kinetics.

The reaction rate[1] was evaluated by using a pseudo first-order kinetics model (Equation S1), and the SMX degradation efficiency (*R*%) was calculated using Equation S2:

$$\ln\left(\frac{C_0}{C_t}\right) = kt \qquad \text{S1}$$

$$R\% = \frac{C_0 - C_e}{C_0} \times 100 \qquad \text{S2}$$

Where C_0 is the initial pollutant concentration, C_t is the concentration at a certain time t during the degradation process, C_e is the adsorbate concentration at equilibrium, and k is the reaction rate constant.

Text S4. ROS concentration measurement.

DPBF was employed as a $^1O_2$ trapping agent was employed to analyze the $^1O_2$ concentration.[2] The $^1O_2$ concentration was obtained from the concentration of the degraded DPBF (molar ratio 1:1), measured by using a UV-Vis spectrometer at λ = 410 nm. BA was used as a molecular probe to detect the $HO^{\bullet}$ concentration, analyzed by the concentration of the byproduct (p-hydroxybenzoic acid, p-HBA), as per the equation: $[HO^{\bullet}] = [p\text{-}HBA] \times 5.87$. The p-HBA concentration was measured by HPLC, with the mobile phase consisting of water/acetonitrile (85/15, v/v) at λ = 270 nm. In addition, the amount of generated $SO_4^{\bullet-}$ was quantified by measuring the indirect product of benzoquinone, resulting due to the $SO_4^{\bullet-}$ oxidation of p-HBA. The benzoquinone concentration was measured by HPLC, with the mobile phase consisting of methanol/water (50/50, v/v) at λ = 244 nm.

Text S5. Energy consumption.

The electric energy (kWh m^{-3})[3] normalized per log-removal of contaminant was calculated using Equation S3:

$$E = 10^{-3} \times \frac{V I}{Q \log(\frac{C_0}{C_e})} \qquad \text{S3}$$

Where I is the current (mA), V is the total cell potential (V), and Q is the volumetric flow rate (m^3 h^{-1}).

Table S1. EXAFS fitting parameters at the Cu K-edge (S_0^2 = 0.85).

Sample	Shell	N^a	R(Å)^b	$\sigma^2\times10^3$(Å^2)^c	ΔE_0 (eV)^d	R factor
Cu-SA/$Ti_3C_2T_x$	Cu–O	3.1 ± 0.3	1.5	11.9	4.3 ± 0.7	0.018

$^a N$: coordination numbers; $^b R$: bond distance; $^c \sigma^2$: Debye-Waller factors; $^d \Delta E_0$: the inner potential correction. R factor: goodness of fit.

Table S2. Comparison of different catalysts for micro-pollutants removal.

No.	Name	Type	Pollutant (mg L^{-1})	Time	pH	Removal efficiency	*k*-value (min^{-1})	Total cell potential (V)	Energy consumption (kWh m^{-3})	Refer.
1	$CoFe_2O_4$ nanoparticles	Metal oxide hybrids	SMX (10)	20 min	6	99%	0.293			4
2	Co_3O_4-Bi_2O_3 nanoparticles	Metal oxide nanoparticles	BPA (20)	30 min	7	98%	0.441			5
3	Zr-doped Ir Anode	Electrochemistry	SMX (20)	120 min		100%		4	8.50	6
5	CNT/r-FeOOH cathode	Bio-electro-Fenton system	SMX (25)			94.6%		0.23	0.28	7
6	Ti/Ta_2O_5-SnO_2 electrodes	Electrochemical	CBZ (20)	480 min	7	71.7%	1.57		60.30	8
7	FeS_2@BrGO	Electro-Fenton	BPA (50)	20 min	7.4		0.58	4.5		9

8	Cu-NC/$Ti_3C_2T_x$ cathode	Electrochemistry	SMX (10)		6.1	77.9%	0.15	1	1.13	This work
9	Cu-NP/$Ti_3C_2T_x$ cathode	Electrochemistry	SMX (10)		6.2	67.1%	0.06	1	2.26	This work
10	**Cu-SA/$Ti_3C_2T_x$ cathode**	**Electrochemistry**	**SMX (10)**	143.8 ms	**6.2**	**100%**	**3.19**	**1**	**0.37**	**This work**

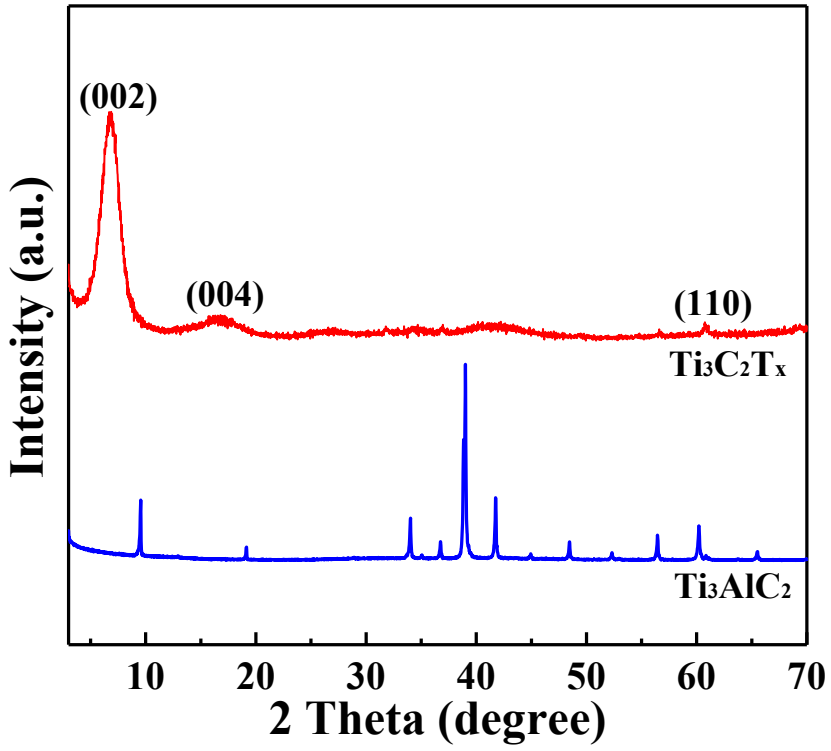

Figure S1. XRD patterns of Ti_3AlC_2 powder and $Ti_3C_2T_x$ nanohybrid filter.

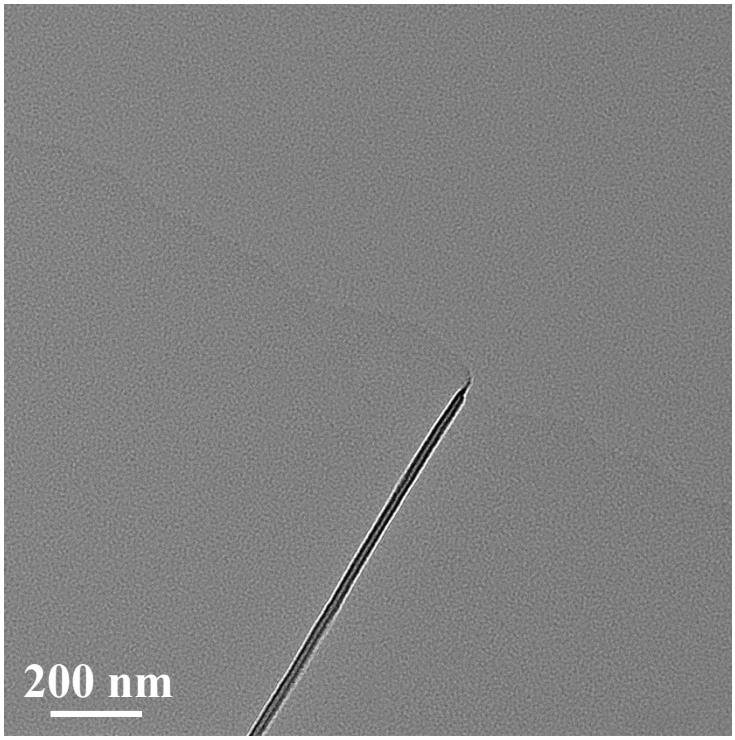

Figure S2. FETEM image of $Ti_3C_2T_x$.

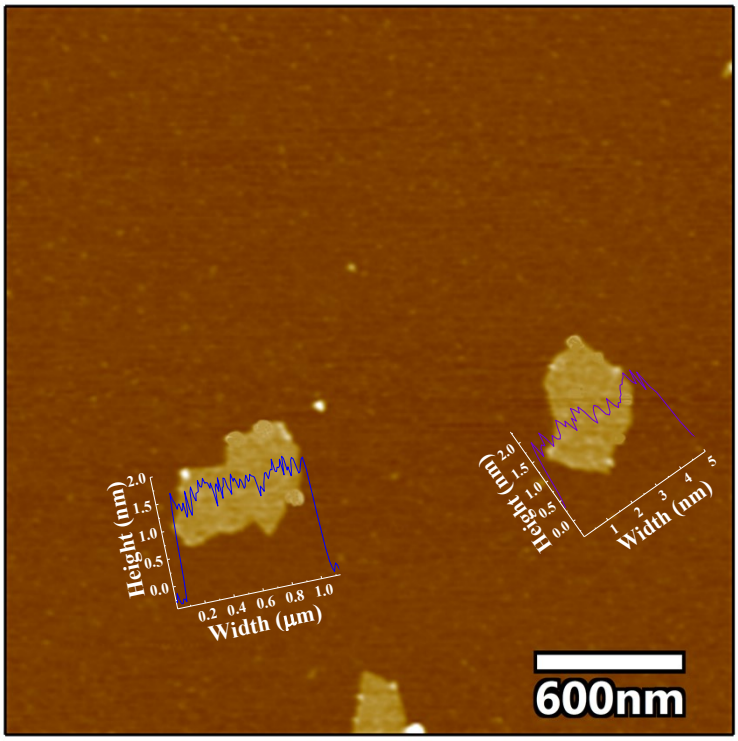

Figure S3. AFM image of the $Ti_3C_2T_x$ nanohybrid filter on cleaved mica.

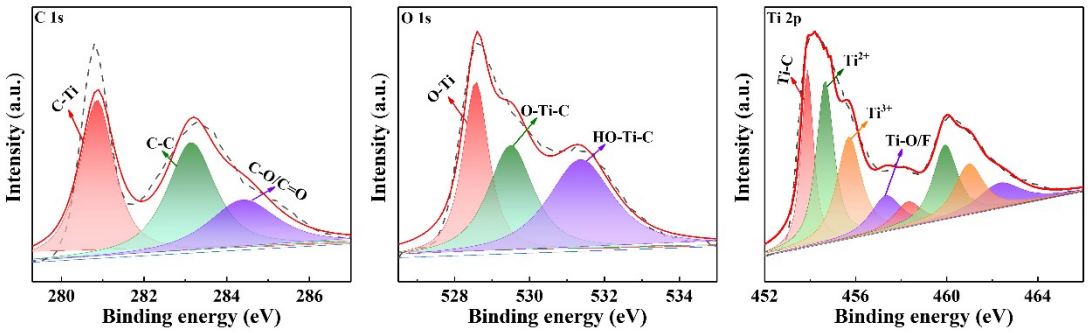

Figure S4. XPS spectra of the $Ti_3C_2T_x$ nanohybrid filter.

Note: The peaks that correspond to C−Ti, O−Ti, C−Ti−O/OH, C−C and C−O/C=O bonds were deconvoluted.[10] The Ti 2p spectrum of $Ti_3C_2T_x$ membrane contains four main sets of peaks corresponding to (i) Ti–C bonds at binding energies of 454.0 eV, (ii) Ti^{2+} suboxides and/or hydroxides (454.6 eV), (iii) Ti^{3+} suboxides and/or hydroxides (455.6 eV), and (iv) a weak peak attributed to Ti–O/F groups (457.6 eV), suggesting accessible surface-terminating (O, OH and F) groups on the MXene nanosheets.[11]

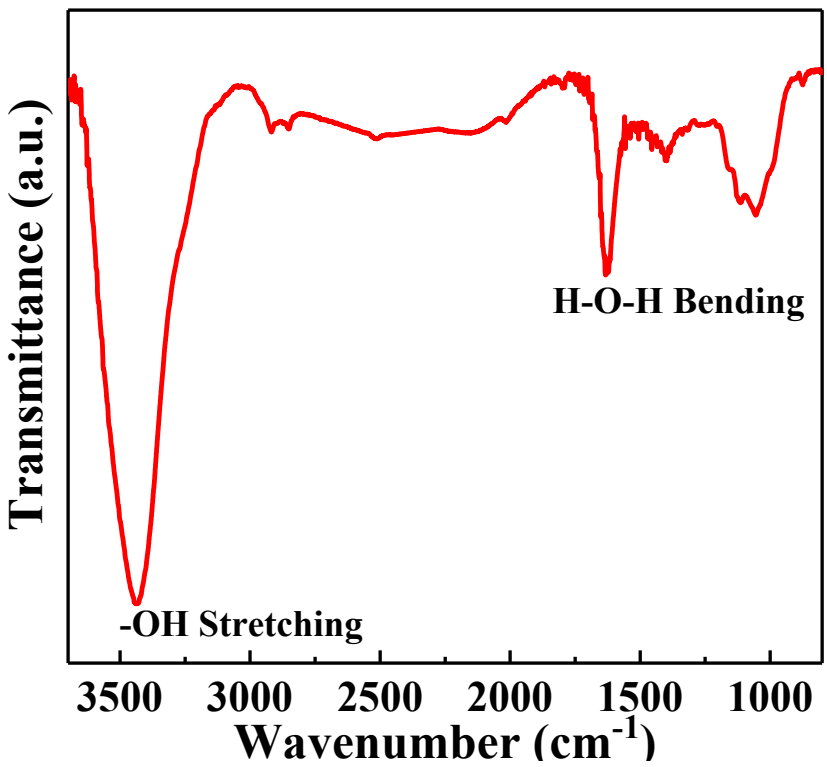

Figure S5. FTIR spectra of the $Ti_3C_2T_x$ nanohybrid filter.

Note: the FTIR spectrum of $Ti_3C_2T_x$ nanohybrid filter exhibited two typical representative peaks at 3445 cm^{-1} and 1645 cm^{-1}, corresponding to the vibration of O–H stretching and H–O–H bending on the $Ti_3C_2T_x$ nanohybrid filter.[12]

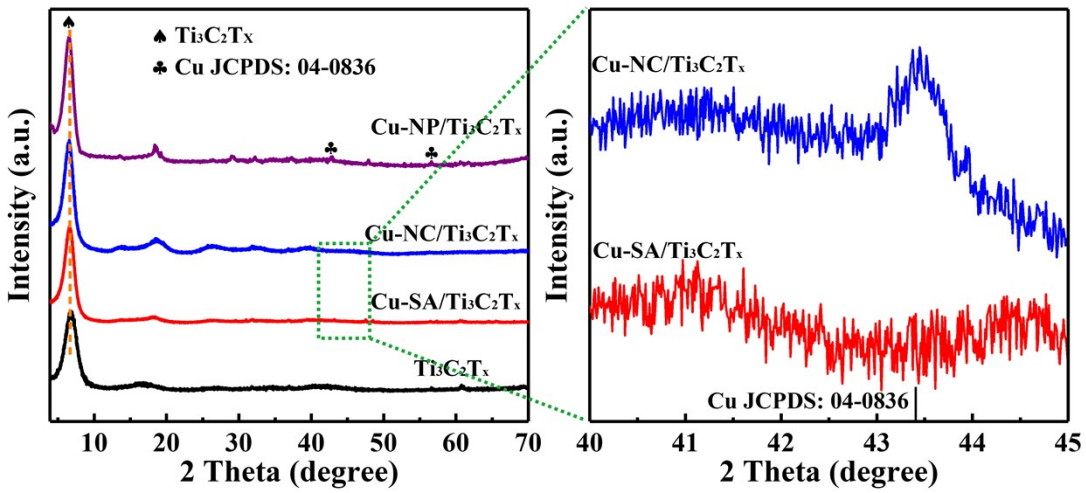

Figure S6. XRD patterns of the $Ti_3C_2T_x$, Cu-SA/$Ti_3C_2T_x$, Cu-NC/$Ti_3C_2T_x$ and Cu-NP/$Ti_3C_2T_x$ nanohybrid filters.

Note: In the XRD pattern of Cu-NC/$Ti_3C_2T_x$ (Figure S5), a distinct peak at 43.4° were observed, corresponding to the respective {111} crystal plane of Cu NC.[13] In contrast, no XRD peak was observed for Cu-SA/$Ti_3C_2T_x$. As such, the size of Cu species in Cu-SA/$Ti_3C_2T_x$ is below the detection limit of XRD and TEM, possibly in the Cu-SA regime.

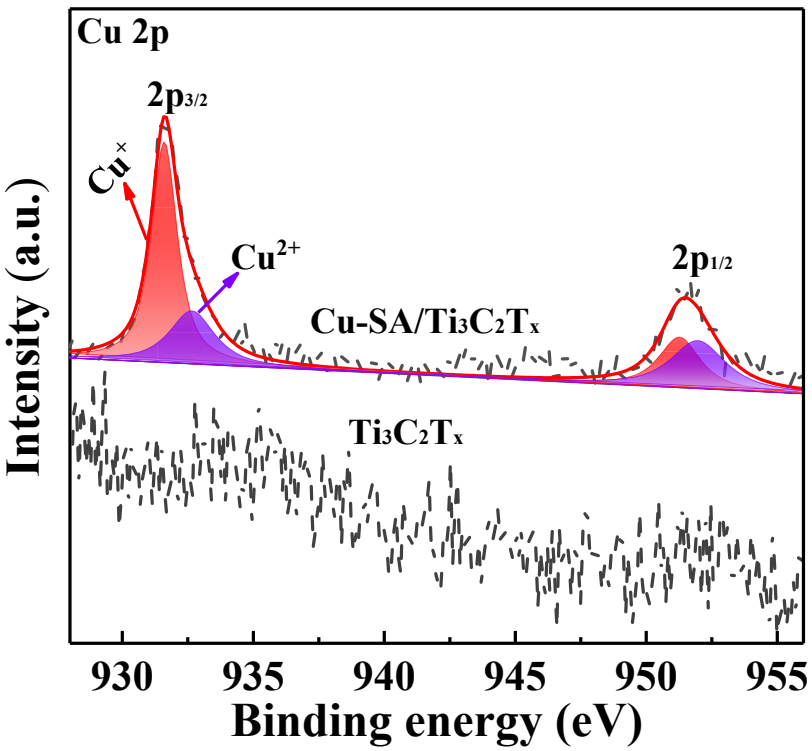

Figure S7. XPS spectra of Cu-SA/$Ti_3C_2T_x$ and pure $Ti_3C_2T_x$ nanohybrid filters.

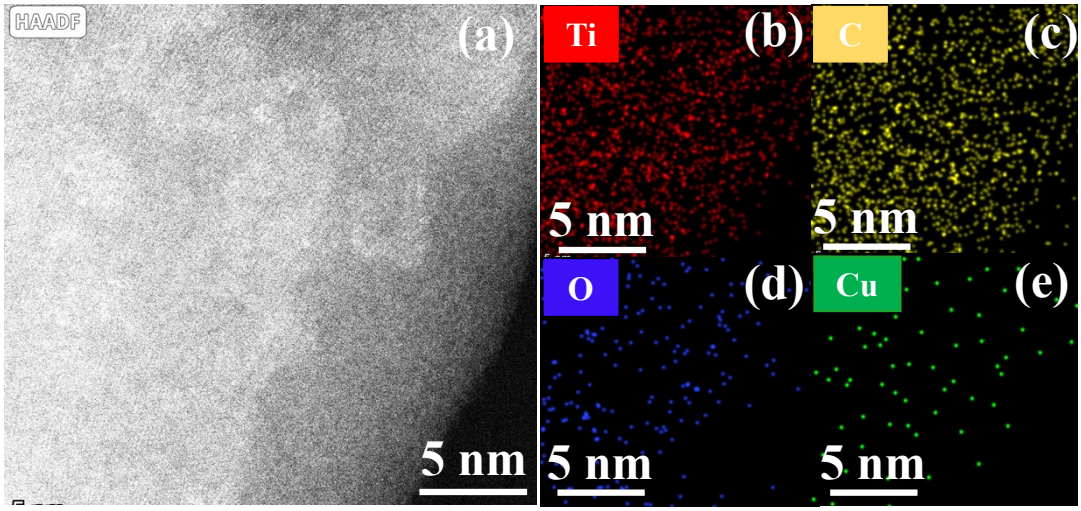

Figure S8. The EDX elemental mappings of Cu-SA/$Ti_3C_2T_x$. HAADF-STEM image (a) and the corresponding EDX elemental mapping images of Cu-SA/$Ti_3C_2T_x$ filter: (b) Ti, (c) C, (d) O and (e) Cu.

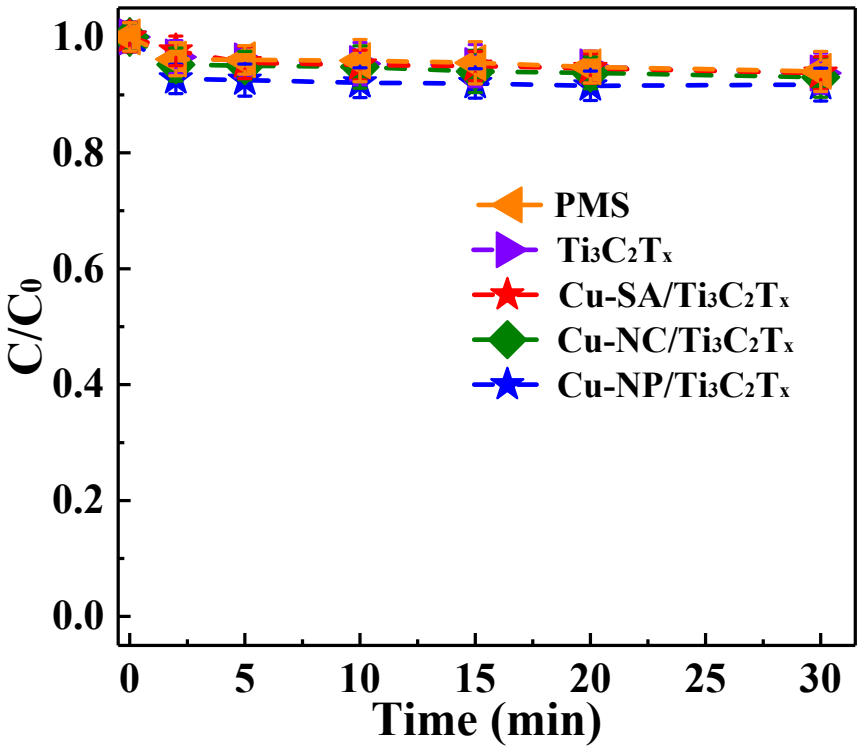

Figure S9. The SMX removal by PMS, pure $Ti_3C_2T_x$, Cu-SA/$Ti_3C_2T_x$, Cu-NC/$Ti_3C_2T_x$ and Cu-NP/$Ti_3C_2T_x$ nanohybrid filters alone. Experimental condition: $[PMS]_0$ = 1.5 mmol L^{-1}, $[SMX]_0$ = 0.04 mmol L^{-1}, flow velocity = 1.5 mL min^{-1}, total cell potential = 1 V, and pH = 6.2 ± 0.2.

Note: PMS alone exhabited a very weak oxidation (<3%) on SMX removal, suggesting that the activation of PMS should be ignored. Besides, pure $Ti_3C_2T_x$, Cu-SA/$Ti_3C_2T_x$, Cu-NC/$Ti_3C_2T_x$ and Cu-NP/$Ti_3C_2T_x$ nanohybrid filters alone showed a negligible adsorption (5%) of SMX within 30 min in a single-pass model.

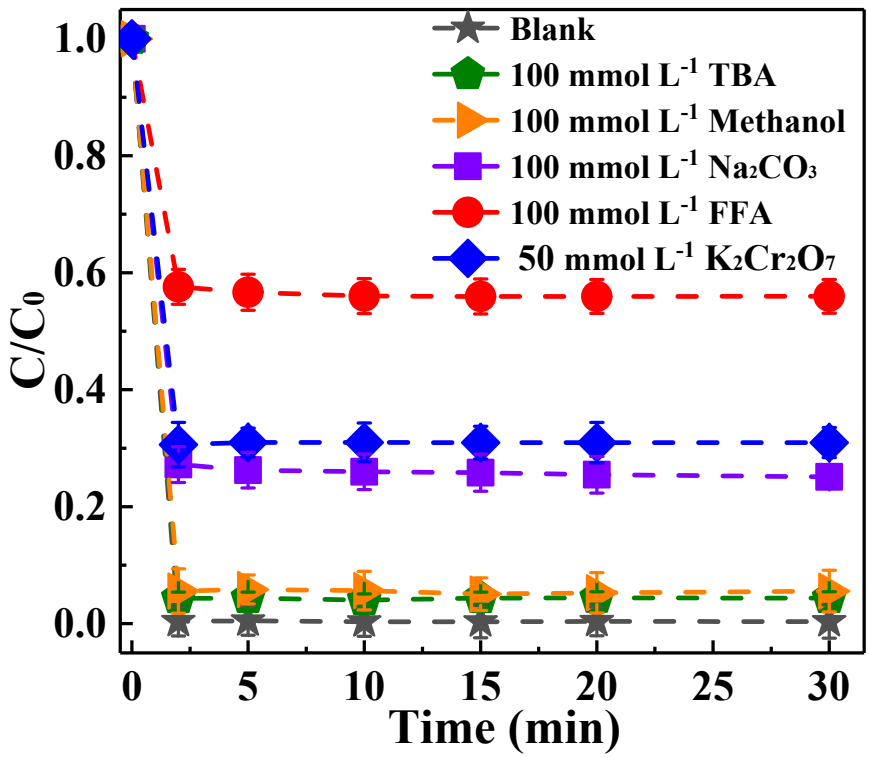

Figure S10. Effect of different quenching agents on the SMX degradation. Experimental condition: $[PMS]_0$ = 1.5 mmol L^{-1}, $[SMX]_0$ = 0.04 mmol L^{-1}, flow velocity = 1.5 mL min^{-1}, total cell potential = 1 V, and pH = 6.2 ± 0.2.

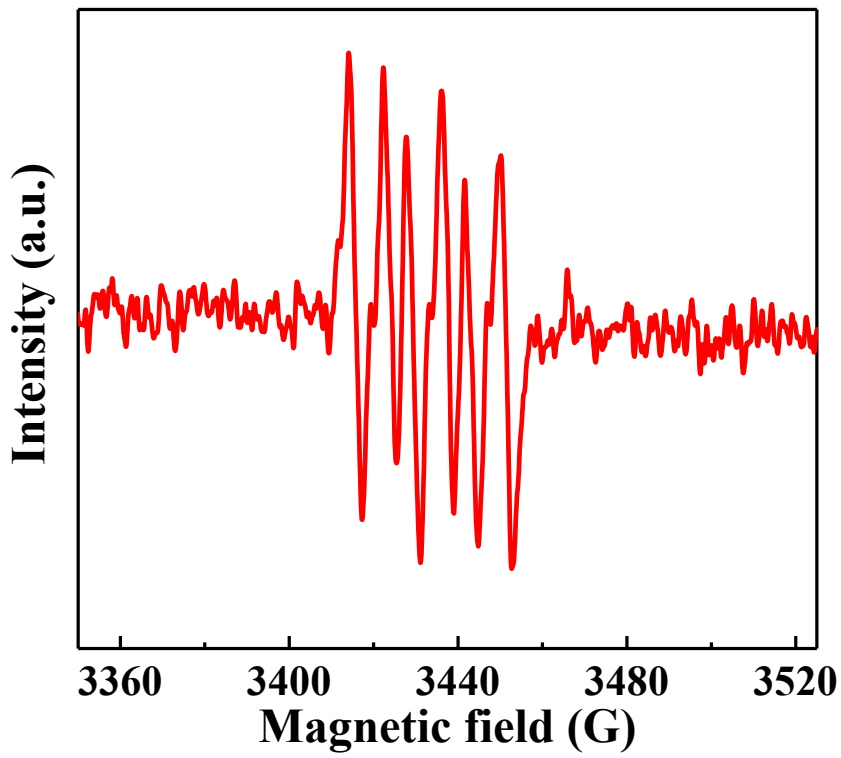

Figure S11. EPR spectra with DMPO in methanol solution. Experimental condition: $[PMS]_0$ = 1.5 mmol L^{-1}, flow velocity = 1.5 mL min^{-1}, total cell potential = 1 V, and pH = 6.2 ± 0.2.

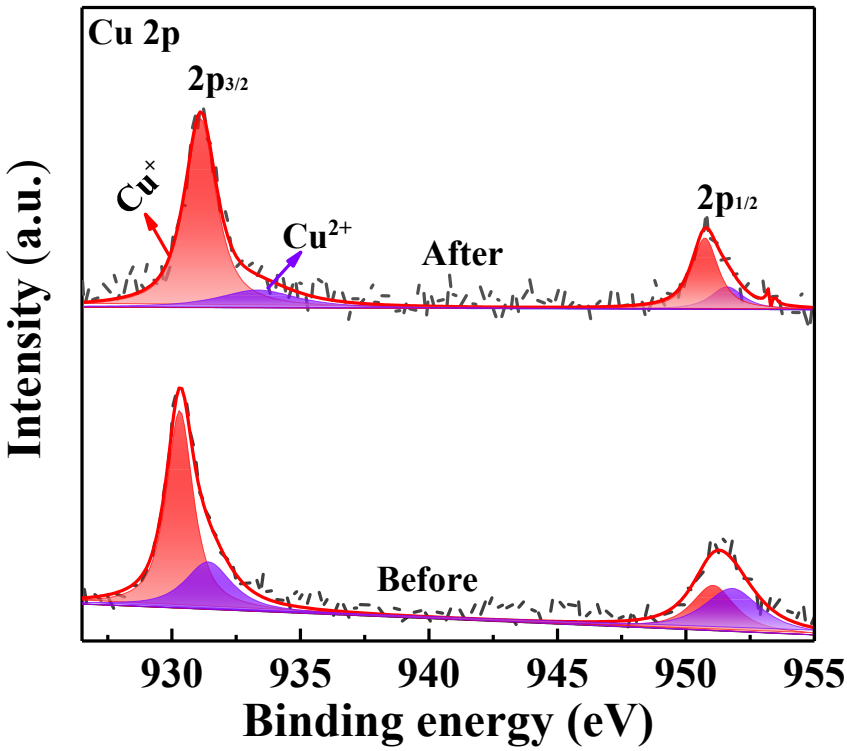

Figure S12. XPS spectra of Cu 2p of Cu-SA/$Ti_3C_2T_x$ nanohybrid filter before and after reaction.

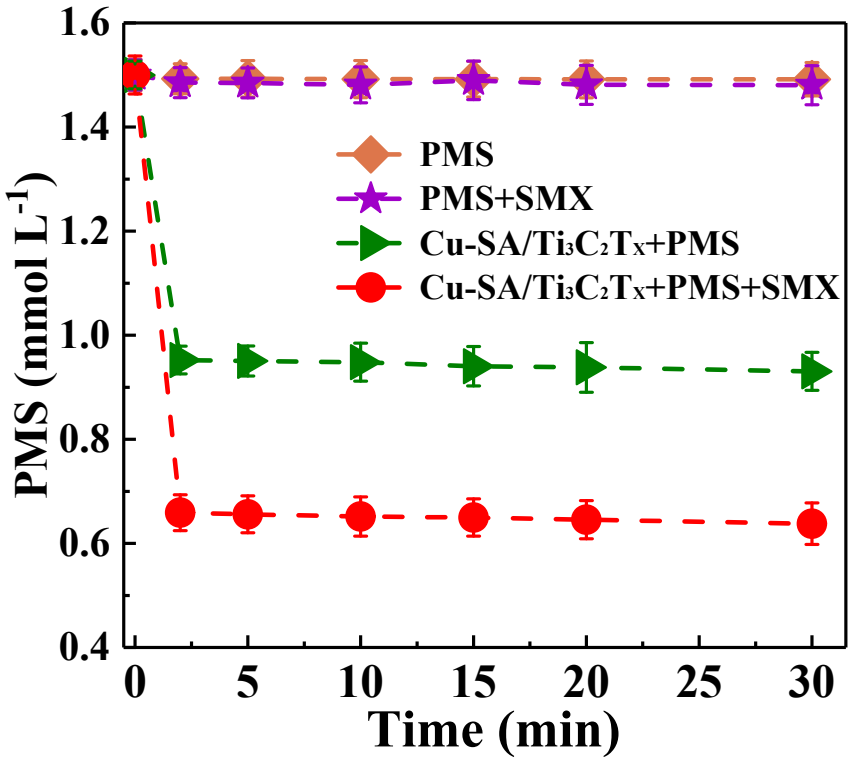

Figure S13. PMS decomposition under different conditions. Experimental condition: $[PMS]_0$ = 1.5 mmol L^{-1}, $[SMX]_0$ = 0.04 mmol L^{-1}, flow velocity = 1.5 mL min^{-1}, total cell potential = 1 V, and pH = 6.2 ± 0.2.

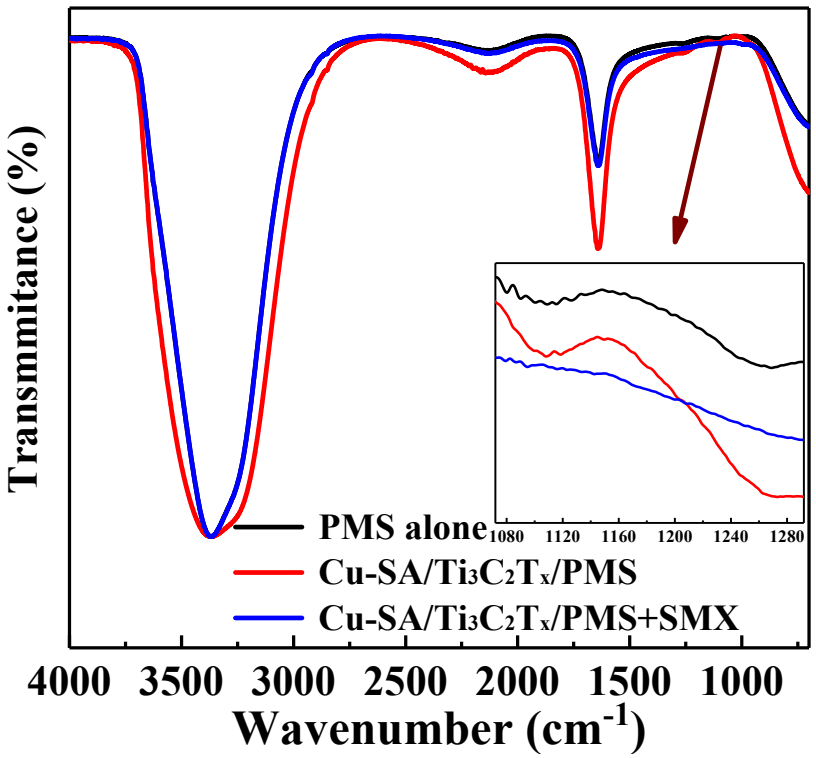

Figure S14. ATR-FTIR spectra of the alone PMS solution, PMS pass through Cu-SA/$Ti_3C_2T_x$ nanohybrid filter, PMS and SMX pass through Cu-SA/$Ti_3C_2T_x$ filter together. Experimental condition: $[PMS]_0$ = 1.5 mmol L^{-1}, $[SMX]_0$ = 0.04 mmol L^{-1}, flow velocity = 1.5 mL min^{-1}, total cell potential = 1 V, and pH = 6.2 ± 0.2.

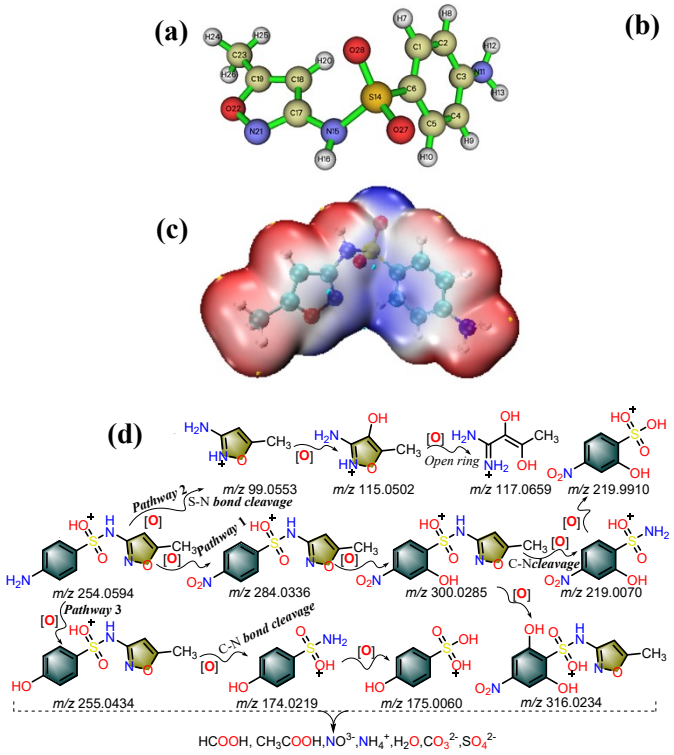

(b)

Atom	charge(0) e/a.u.	charge(+1) e/a.u.	charge(-1) e/a.u.	f^-
1(C)	-0.16572	-0.09835	-0.09048	0.0289
2(C)	-0.25256	-0.04932	-0.13208	0.0575
3(C)	0.20973	0.14201	0.08691	0.044
4(C)	-0.24543	-0.05439	-0.13079	0.0478
5(C)	-0.14842	-0.09724	-0.08347	0.0287
6(C)	-0.32867	-0.05105	-0.10097	0.0559
7(H)	0.23381	0.12288	0.11321	0.0211
8(H)	0.20231	0.11116	0.09102	0.0295
9(H)	0.20272	0.112	0.09168	0.0278
10(H)	0.22327	0.12486	0.11437	0.021
11(N)	-0.75193	-0.21686	-0.39116	0.1055
12(H)	0.36985	0.19967	0.17287	0.0379
13(H)	0.36996	0.19937	0.17257	0.0385
14(S)	2.21858	1.10942	0.93849	0.0226
15(N)	-0.83825	-0.25198	-0.19376	0.0494
16(H)	0.41675	0.21459	0.15473	0.024
17(C)	0.3411	0.1609	0.12655	0.02
18(C)	-0.36789	-0.1805	-0.15909	0.0096
19(C)	0.37304	0.20205	0.1479	0.0367
20(H)	0.23162	0.13352	0.10705	0.0067
21(N)	-0.18888	0.09081	-0.03519	0.0806
22(O)	-0.32193	-0.10817	-0.16993	0.0408
23(C)	-0.60785	-0.31032	-0.2981	0.0138
24(H)	0.22008	0.12187	0.0979	0.0192
25(H)	0.21285	0.11544	0.09987	0.0108
26(H)	0.21861	0.12016	0.10003	0.0182
27(O)	-0.9153	-0.42247	-0.41794	0.0552
28(O)	-0.91146	-0.44007	-0.4086	0.0482

Figure S15. The chemical structure of SMX (a), NPA charge distribution and Fukui index of SMX (b), ESP map of SMX (c), and possible routes of degradation of SMX in the Cu-SA/$Ti_3C_2T_x$ system (d). Experimental condition: $[PMS]_0$ = 1.5 mmol L^{-1}, $[SMX]_0$ = 0.04 mmol L^{-1}, flow velocity = 1.5 mL min^{-1}, total cell potential = 1 V, and pH = 6.2 ± 0.2.

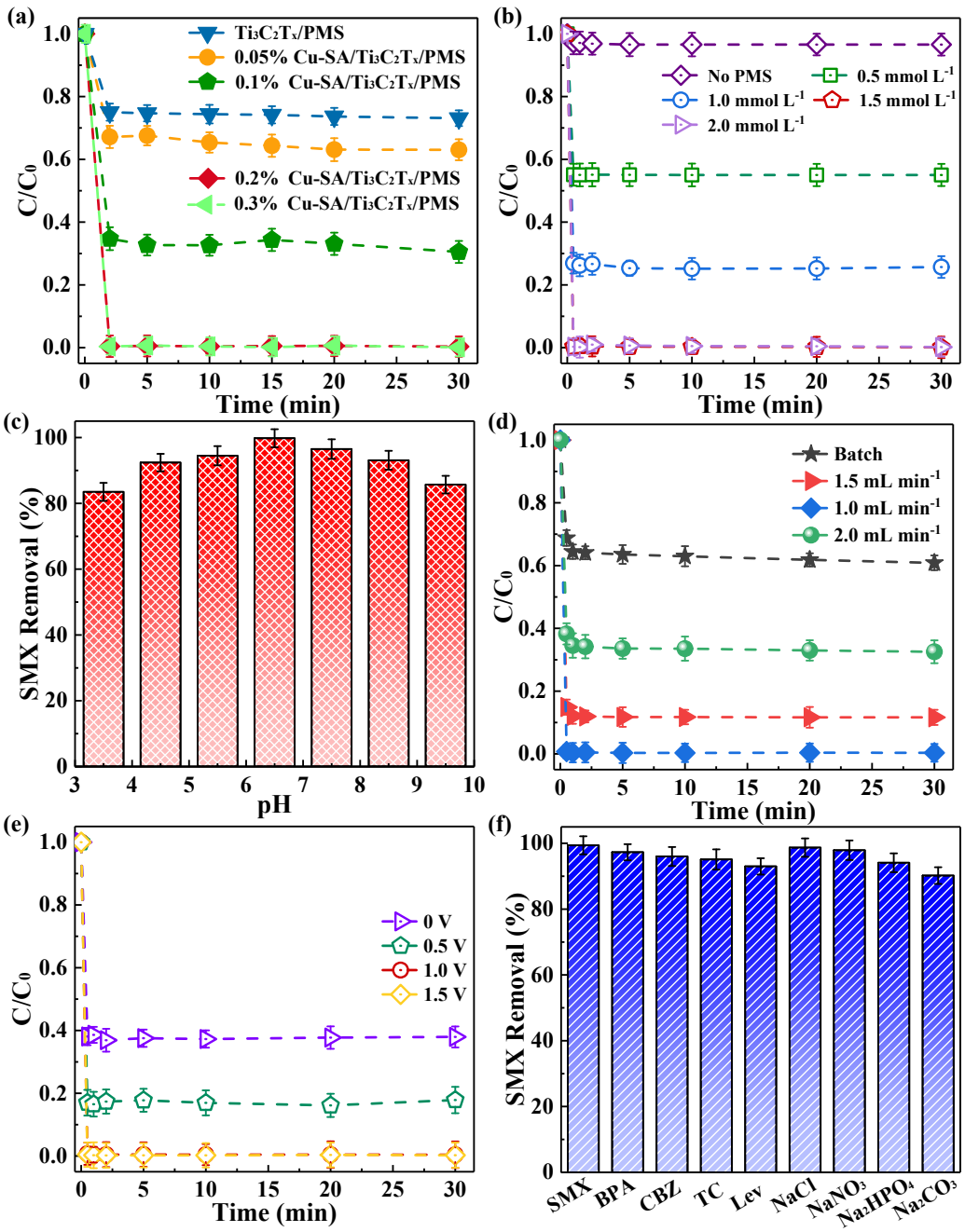

Figure S16. Effect of the loading of Cu-SA (a), PMS dose(b), initial pH (c), flow velocity (c), applied total cell potential (e) and coexisting micropollutant and salts (f) for Cu-SA/$Ti_3C_2T_x$ nanohybrid filter in the single-pass filtration mode. Experimental conditions: $[PMS]_0$ = 1.5 mmol L^{-1}, $[SMX]_0$ = $[BPA]_0$ = $[CBZ]_0$ = $[TC]_0$ = $[Lev]_0$ = 0.04 mmol L^{-1}, $[NaCl]_0$ = $[NaNO_3]_0$ = $[Na_2HPO_4]_0$ = $[Na_2CO_3]_0$ = 10 mmol L^{-1}, flow velocity = 1.5 mL min^{-1}, total cell potential = 1 V, and pH = 6.2 ± 0.2.

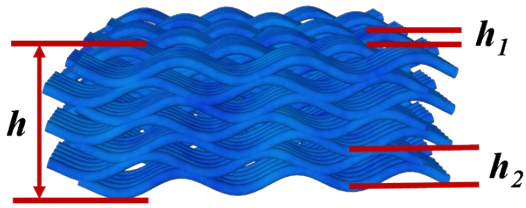

Figure S17. Estimation of retention time of Cu-SA/$Ti_3C_2T_x$ nanohybrid filter.

Note: we treat the membrane as an ideal filter with uniform thickness of nanosheets, and interspacing.[14] The approximate calculation of retention times was illustrated as followed (Equation S1, S2).

$$t = \frac{V}{Q} = \frac{S_{Area} \times h'}{Permeance \times S_{Area} \times Pressure} = \frac{h'}{Permeance \times Press} \quad \text{(S1)}$$

$$h' = h_2\left(\frac{h + h_2}{h_1 + h_2} - 1\right) = h_2\left(\frac{h - h_1}{h_1 + h_2}\right) \approx \frac{h_2 h}{h_1 + h_2} \quad \text{(S2)}$$

Where h, h_1 and h_2 represents for the thickness of membrane, $Ti_3C_2T_x$ nanosheet and interspacing, respectively (nm). S_{Area} (cm^2) stands for the effective filter area of membrane. *Permeance* (L $(m^2 \cdot h \cdot bar)^{-1}$) and *Pressure* (bar) could be obtained by experiments conditions. In an ideal condition, the measurements of h, h_1 and h_2 should be obtained via cross-sectional FESEM, AFM images and results from Bragg's Law ($2d \cdot \sin\vartheta = n\lambda$), respectively. Notably, the spacing of (002) plane corresponds to the interspacing of membranes.

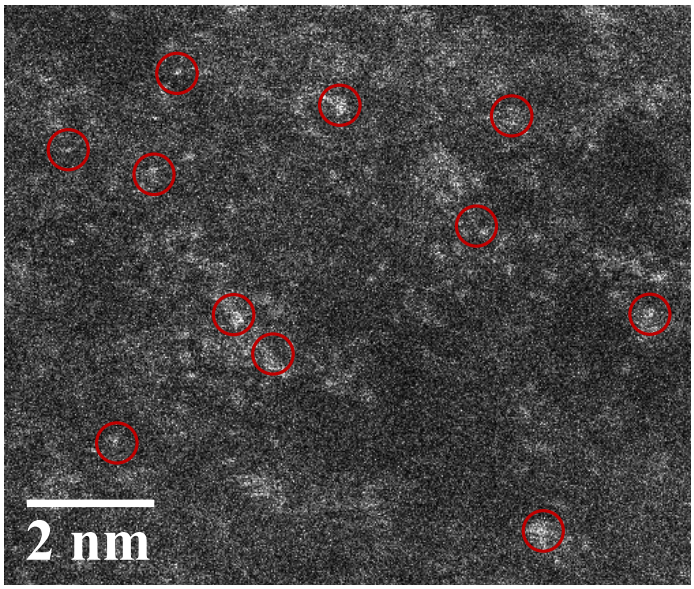

Figure S18. The atomic-resolution HAADF-STEM images of the Cu-SA/$Ti_3C_2T_x$ nanohybrid filter after stability test.

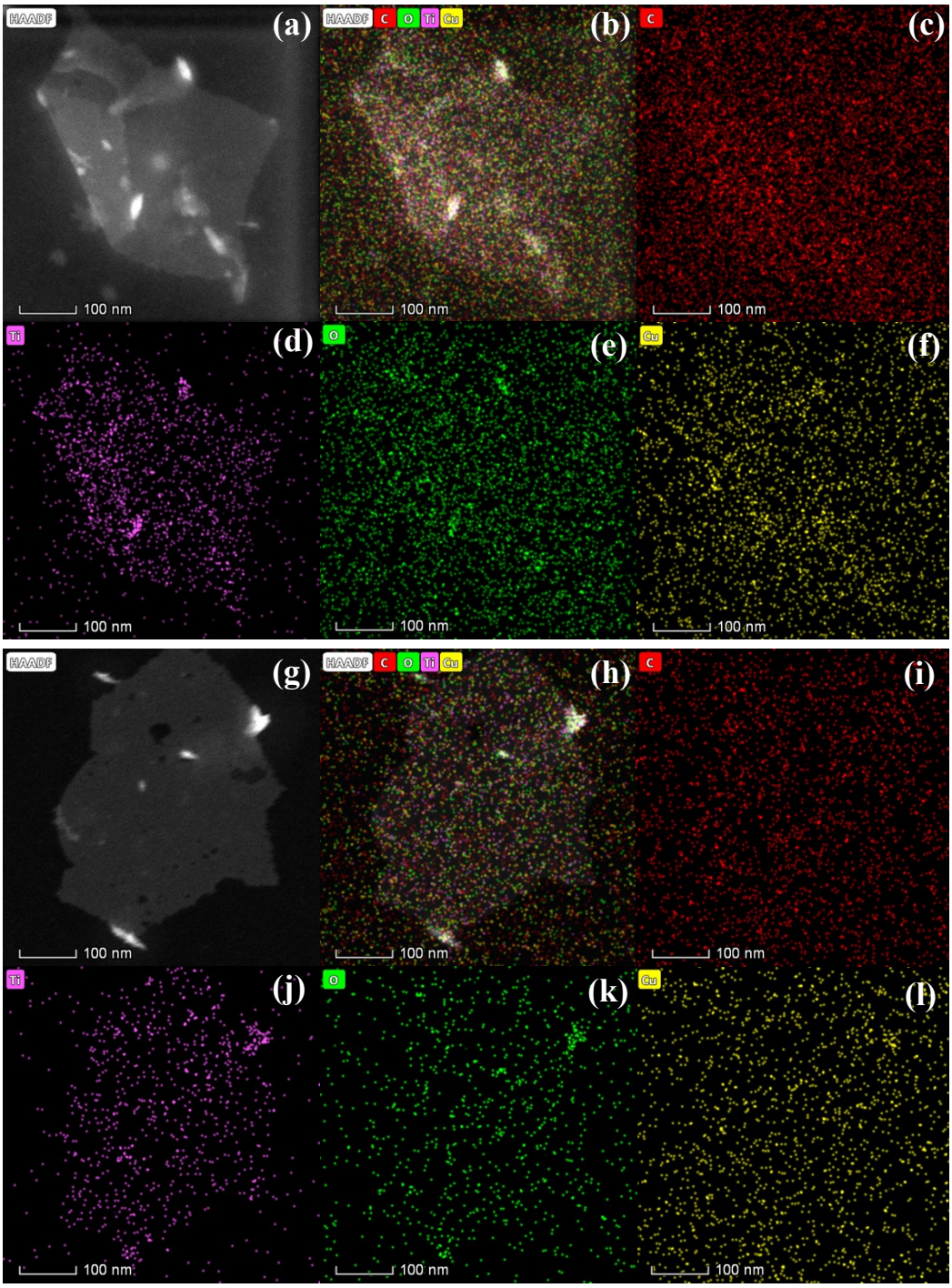

Figure S19. HAADF-STEM and EDS mapping on the Cu-SA/$Ti_3C_2T_x$ nanohybrid filter before (a-f) and after (g-l) tests.

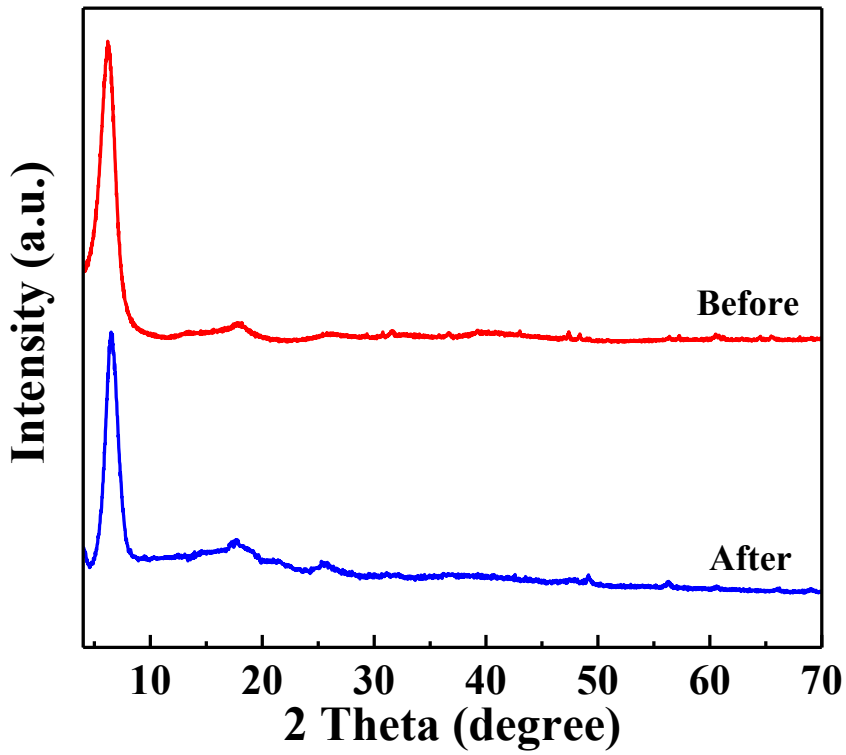

Figure S20. XRD patterns of the Cu-SA/$Ti_3C_2T_x$ nanohybrid filter before after stability test.

References

1 C. Q. Zhu, S. F. Zhao, Z. W. Fan, H. D. Wu, F. Q. Liu, Z. X. Chen and A. M. Li, *Adv. Funct. Mater.*, 2020, **30**, 2003947.

2 J. J. Jiang, X. Wang, Y. Liu, Y. H. Ma, T. R. Li, Y. H. Lin, T. F. Xie and S. S. Dong, *Appl. Catal. B: Environ.*, 2020, **278**, 119349.

3 T. X. H. Le, H. Haflich, A. D. Shah and B. P. Chaplin, *Environ. Sci. Technol. Lett.*, 2019, **6**, 504-510.

4 M. J. Xu, J. Li, Y. Yan, X. G. Zhao, J. F. Yan, Y. H. Zhang, B. Lai, X. Chen and L. P. Song, *Chem. Eng. J.*, 2019, **369**, 403-413.

5 L. M. Hu, G. S. Zhang, M. Liu, Q. Wang, S. Y. Dong and P. Wang, *Sci. Total Environ.*, 2019, **647**, 352-361.

6 F. Q. Xiong, D. N. Chen, C. L. Ma, L. M. Cao and J. Yang, *ACS Omega*, 2020, **5**, 3358-3364.

7 S. N. Li, T. Hua, C. S. Yuan, B. k. Li, X. Y. Zhu and F. X. Li, *Bioresour. Technol.*, 2020, **298**, 122501.

8 K. Gurung, M. C. Ncibi, M. Shestakova and M. Sillanpää, *Appl. Catal. B: Environ.*, 2018, **221**, 329-338.

9 L. G. Chu, Z. Y. Sun, G. D. Fang, L. Cang, X. H. Wang, D. M. Zhou and J. Gao, *Sep. Purif. Technol.*, 2021, **267**, 118680.

10 J. Halim, K. M. Cook, M. Naguib, P. Eklund, Y. Gogotsi, J. Rosen and M. W. Barsoum, *Appl. Surf. Sci.*, 2016, **362**, 406-417.

11 L. Ding, Y. Y. Wei, L. Li, T. Zhang, H. Wang, J. Xue, L. X. Ding, S. Q. Wang, J. Caro and Y. Gogotsi, *Nat. Commun.*, 2018, **9**, 155.

12 J. T. Wang, P. P. Chen, B. B. Shi, W. W. Guo, M. Jaroniec and S. Z. Qiao, *Angew. Chem. Int. Ed.*, 2018, **57**, 6814-6818.

13 X. H. Kang, Z. B. Mai, X. Y. Zou, P. X. Cai and J. Y. Mo, *Anal. Biochem.*, 2007, **363**, 143-150.

14 Y. Chen, G. Zhang, H. J. Liu and J. H. Qu, *Angew. Chem. Int. Ed.*, 2019, **58**, 8134-8138.